arXiv:cond-mat/0610163v1 [cond-mat.str-el] 5 Oct 2006

# Electronic spectrum in high-temperature cuprate superconductors

N.M.Plakida[a,b] and V.S. Oudovenko[a,c]
[a] *Joint Institute for Nuclear Research, 141980 Dubna, Russia*
[b] *Max-Planck-Institut für Physik komplexer Systeme, D-01187 Dresden, Germany*
[c] *Rutgers University, Piscataway, New Jersey 08854, USA*

A microscopic theory for electronic spectrum of the $CuO_2$ plane within an effective $p$-$d$ Hubbard model is proposed. Dyson equation for the single-electron Green function in terms of the Hubbard operators is derived which is solved self-consistently for the self-energy evaluated in the noncrossing approximation. Electron scattering on spin fluctuations induced by kinematic interaction is described by a dynamical spin susceptibility with a continuous spectrum. Doping and temperature dependence of electron dispersions, spectral functions, the Fermi surface and the coupling constant $\lambda$ are studied in the hole doped case. At low doping, an arc-type Fermi surface and a pseudogap in the spectral function are observed.

PACS numbers: 74.20.Mn, 71.27.+a, 71.10.Fd, 74.72.-h

## I. INTRODUCTION

Recent high-resolution angle-resolved photoemission spectroscopy (ARPES) studies revealed a complicated character of electronic structure and quasiparticle (QP) spectra in copper oxide superconductors. In particular, a pseudogap in the electronic spectrum and an arc-type Fermi surface (FS) at low hole concentrations were revealed, a substantial wave-vector and energy dependent renormalization of the Fermi-velocity of QP ("kinks" in the dispersion) was observed (see, e.g.,[1,2,3] and references therein). As was originally pointed out by Anderson[4], strong electron correlations in cuprates play an essential role in explaining their normal and superconducting properties.

A conventional approach in describing strong electron correlations is based on consideration of the Hubbard model[5]. The model has some advantages in comparison with the $t$-$J$ model which can be derived from the Hubbard model in the limit of strong correlations. Namely, the Hubbard model allows to study a moderate correlation limit observed experimentally in curates and more consistently takes into account a two-subband character of electronic structure, in particular, a weight transfer between subbands with doping.

Various methods were proposed to study electronic structure within the Hubbard model. An unbiased method based on numerical simulations for finite clusters (for a review see e.g.,[6]) precludes, however, to study subtle features of QP spectra due to poor energy and wave-vector resolutions in small size clusters. In analytical calculations of spectra mean-field type approximations are often used (for a review see[7,8]) which cannot reproduce the above mentioned effects caused by the self-energy contributions. In the dynamical mean field theory (DMFT) (for a review see[9,10]) the self-energy is treated in the single-site approximation which also unable to describe wave-vector dependent phenomena. To overcome this flaw of DMFT, various types of the dynamical cluster theory were developed (for a review see[11,12]). In these methods only a restricted wave-vector and energy resolutions can be achieved, depending on the size of the clusters, while the physical interpretation of the origin of an anomalous electronic structure in numerical methods is not straightforward.

To elucidate the mechanism of the pseudogap formation, the charge carriers scattering by short-ranged (static) antiferromagnetic (AF) spin fluctuations was considered in several analytical semi-phenomenological studies (for a review see[2]). More recently, by including into the DMFT scheme an additional momentum-dependent component of the self-energy originating from short-range AF (or charge) correlations, the spin-fluctuation scenario of the pseudogap formation[13] and the arc-type FS[14] have been supported (for a review see[15]). At the same time, it is important to study the effects of the charge carriers scattering by the *dynamical* spin-fluctuations which are believed to be responsible for the kink phenomenon[3]. This can be done by considering the Dyson equation for the single-particle Green function (GF) within the Hubbard model in the limit of strong correlations. For instance, calculation of electronic spectrum within the first order perturbation theory for the self-energy has reproduced quite accurately quantum Monte Carlo results[16], while application of an incremental cluster expansion for the self-energy has enabled to observe a kink structure in the QP spectrum[17].

The aim of the present paper is to develop a microscopic theory for the electronic spectrum in strongly correlated systems, as cuprates, which consistently takes into account effects of electron scattering by dynamical spin fluctuations. For this, we have considered an effective Hubbard model reduced form the $p$-$d$ model for the $CuO_2$ plane in cuprates. By applying the Mori-type projection technique for the thermodynamic GF[18] in terms of the Hubbard operators, we derived an *exact* Dyson equation, as was elaborated in our previous publications[19,20,21]. A self-consistent solution of the Dyson equation with the self-energy evaluated in the noncrossing approximation (NCA) beyond a perturbation approach was performed.

This enabled us to calculate the dispersion and spectral functions of single-particle excitations, the FS, and

the electron occupation numbers. In particular, we studied a hole-doped case at various hole concentrations. At low doping, the FS reveals an arc-type shape with a pseudogap in the $(\pi, 0)$ region of the Brillouin zone (BZ). A strong renormalization effects of the dispersion close to the Fermi energy ("kinks") are observed due to electron scattering by dynamical AF spin fluctuations induced by kinematic interaction generic for the Hubbard operators. Electron occupation numbers show only a small drop at the Fermi energy. For high temperature or large hole concentrations, AF correlations become weak and a crossover to a Fermi-liquid-like behavior is observed.

In the next Section we briefly discuss the model and derivation of the Dyson equation, and the self-energy calculation in the NCA. The results of numerical solution of the self-consistent system of equations for various hole concentrations and discussion are presented in Sect. 3. Conclusion is given in Sect. 4.

## II. GENERAL FORMULATION

### A. Effective Hubbard model and Dyson equation

Following a cell-cluster perturbation theory (e.g.,[19,22,23]) based on a consideration of the original two-band $p$-$d$ model for the $CuO_2$ layer[24] we consider an effective two-dimensional Hubbard model for holes

$$H = \varepsilon_1 \sum_{i,\sigma} X_i^{\sigma\sigma} + \varepsilon_2 \sum_i X_i^{22} + \sum_{i\neq j,\sigma} \{ t_{ij}^{11} X_i^{\sigma 0} X_j^{0\sigma} + t_{ij}^{22} X_i^{2\sigma} X_j^{\sigma 2} + 2\sigma t_{ij}^{12} (X_i^{2\bar{\sigma}} X_j^{0\sigma} + \text{H.c.}) \}, \quad (1)$$

where $X_i^{nm} = |in\rangle\langle im|$ are the Hubbard operators (HOs) for the four states $n, m = |0\rangle, |\sigma\rangle, |2\rangle = |\uparrow\downarrow\rangle$, $\sigma = \pm 1/2 = (\uparrow, \downarrow)$, $\bar{\sigma} = -\sigma$. Here $\varepsilon_1 = \varepsilon_d - \mu$ and $\varepsilon_2 = 2\varepsilon_1 + U_{eff}$ where $\mu$ is the chemical potential. The effective Coulomb energy in the Hubbard model (1) is the charge-transfer energy $U_{eff} = \Delta = \epsilon_p - \epsilon_d$. The superscript 2 and 1 refers to the two-hole $p$-$d$ singlet subband and the one-hole subband, respectively. According to the cell-cluster perturbation theory, we can take similar values for the hopping parameters in (1): $t_{ij}^{22} = t_{ij}^{11} = t_{ij}^{12} = t_{ij}$. The bare electron dispersion defined by the hopping parameter $t_{ij}$ we determine by the conventional equation

$$t(\mathbf{k}) = 4t\,\gamma(\mathbf{k}) + 4t'\,\gamma'(\mathbf{k}) + 4t''\,\gamma''(\mathbf{k}), \quad (2)$$

where $t$, $t'$, $t''$ are the hopping parameters for the nearest neighbor (n.n.) $(\pm a_x, \pm a_y)$, the next nearest neighbor (n.n.n.) $\pm(a_x \pm a_y)$ and $\pm 2a_x, \pm 2a_y$ sites, respectively, and $\gamma(\mathbf{k}) = (1/2)(\cos k_x + \cos k_y)$, $\gamma'(\mathbf{k}) = \cos k_x \cos k_y$ and $\gamma''(\mathbf{k}) = (1/2)(\cos 2k_x + \cos 2k_y)$ (the lattice constants $a_x = a_y$ equal to unity). To get a physically reasonable value for the charge-transfer gap for the conventional value of $t \simeq 0.4$ eV we take $\Delta = U_{eff} = 8\,t \simeq 3.2$ eV. The bare bandwidth is $W = 8t \simeq U_{eff}$ which shows that the effective $p$-$d$ Hubbard model (1) corresponds to the strong correlation limit. In what follows, the energy will be measured in unit of $t$ with $\varepsilon_d = 0$ in $\varepsilon_1$. The chemical potential $\mu$ depends on the average *hole* occupation number

$$n = 1 + \delta = \langle \sum_\sigma X_i^{\sigma\sigma} + 2X_i^{22} \rangle. \quad (3)$$

The HOs entering (1) obey the completeness relation $X_i^{00} + X_i^{\uparrow\uparrow} + X_i^{\downarrow\downarrow} + X_i^{22} = 1$ which rigorously preserves the constraint of no double occupancy of any quantum state $|in\rangle$ at each lattice site $i$. Due to the projected character of the HOs, they have complicated commutation relations $\left[X_i^{\alpha\beta}, X_j^{\gamma\delta}\right]_\pm = \delta_{ij} \left(\delta_{\beta\gamma} X_i^{\alpha\delta} \pm \delta_{\delta\alpha} X_i^{\gamma\beta}\right)$, which results in the so-called *kinematic interaction*. The upper sign here refers for the Fermi-like HOs like $X_i^{0\sigma}$ and the lower sign is for the Bose-like ones, like the spin or number operators.

To discuss the electronic structure within the model (1), we introduce a thermodynamic matrix Green function (GF)[18]

$$\hat{G}_{ij\sigma}(t - t') = \langle\langle \hat{X}_{i\sigma}(t) \,|\, \hat{X}_{j\sigma}^\dagger(t') \rangle\rangle = -i\theta(t - t') \langle \{ \hat{X}_{i\sigma}(t)\,,\, \hat{X}_{j\sigma}^\dagger(t') \} \rangle, \quad (4)$$

in terms of the two-component operators $\hat{X}_{i\sigma} = \begin{pmatrix} X_i^{\sigma 2} \\ X_i^{0\bar{\sigma}} \end{pmatrix}$ and $\hat{X}_{i\sigma}^\dagger = (X_i^{2\sigma}\ X_i^{\bar{\sigma}0})$. To calculate the GF (4), we apply the Mori-type projection technique by writing equations of motion for the Heisenberg operators in the form:

$$\hat{Z}_{i\sigma} = [\hat{X}_{i\sigma},\, H] = \sum_j \hat{\varepsilon}_{ij\sigma} \hat{X}_{j\sigma} + \hat{Z}_{i\sigma}^{(ir)}, \quad (5)$$

where the *irreducible* $\hat{Z}$-operator is determined by the orthogonality condition:

$$\langle \{ \hat{Z}_{i\sigma}^{(ir)},\, \hat{X}_{j\sigma}^\dagger \} \rangle = \langle \hat{Z}_{i\sigma}^{(ir)}\, \hat{X}_{j\sigma}^\dagger + \hat{X}_{j\sigma}^\dagger\, \hat{Z}_{i\sigma}^{(ir)} \rangle = 0\,. \quad (6)$$

This defines the frequency matrix

$$\hat{\varepsilon}_{ij} = \langle \{ [\hat{X}_{i\sigma}, H], \hat{X}_{j\sigma}^\dagger \} \rangle\, \hat{Q}^{-1}, \quad (7)$$

where $\hat{Q} = \langle \{ \hat{X}_{i\sigma}, \hat{X}_{i\sigma}^\dagger \} \rangle = \begin{pmatrix} Q_2 & 0 \\ 0 & Q_1 \end{pmatrix}$. The weight factors $Q_2 = \langle X_i^{22} + X_i^{\sigma\sigma} \rangle = n/2$ and $Q_1 = \langle X_i^{00} + X_i^{\bar{\sigma}\bar{\sigma}} \rangle = 1 - Q_2$ in a paramagnetic state depend only on the hole occupation number (3). The frequency matrix (7) determines the QP spectra within the generalized mean field approximation (MFA). The corresponding zero-order GF in MFA reads:

$$\hat{G}_\sigma^0(\mathbf{k}, \omega) = \left( \omega \hat{\tau}_0 - \hat{\varepsilon}(\mathbf{k}) \right)^{-1} \hat{Q}, \quad (8)$$

where $\hat{\tau}_0$ is the unity matrix and we introduced the frequency matrix (7) in the $\mathbf{k}$-representation $\hat{\varepsilon}(\mathbf{k})$. By differentiating the many-particle GF $\langle\langle \hat{Z}_{i\sigma}^{irr}(t) \mid \hat{X}_{j\sigma}^\dagger(t') \rangle\rangle$

over the second time $t'$ and applying the same projection procedure as in (5) we derive the Dyson equation in the form[19]

$$\hat{G}_\sigma(\mathbf{k},\omega)^{-1} = \hat{G}^0_\sigma(\mathbf{k},\omega)^{-1} - \hat{\Sigma}_\sigma(\mathbf{k},\omega). \qquad (9)$$

Here the self-energy matrix $\hat{\Sigma}_\sigma(\mathbf{k},\omega)$ is determined by a *proper* part (which have no single zero-order GF) of the many-particle GF in the form

$$\hat{\Sigma}_\sigma(\mathbf{k},\omega) = \hat{Q}^{-1} \langle\langle \hat{Z}^{(ir)}_\sigma \,|\, \hat{Z}^{(ir)\dagger}_\sigma \rangle\rangle^{(prop)}_{\mathbf{k},\omega} \, \hat{Q}^{-1}. \qquad (10)$$

The equations (8) – (10) provide an exact representation for the GF (4). However, to calculate it one has to use an approximation for the self-energy matrix (10) which describes inelastic scattering of electrons on spin and charge fluctuations.

It is important to point out that in the Hubbard model (1) electron interaction with spin- or charge fluctuations are induced by the kinematic interaction with the coupling constants equal to the original hopping parameters, as has been already pointed out by Hubbard[5]. For instance, the equation of motion for the operator $X^{\sigma 2}_i$ reads

$$\begin{aligned} id\, X^{\sigma 2}_i/dt &= [X^{\sigma 2}_i, H] = (\varepsilon_1 + \Delta) X^{\sigma 2}_i \\ &+ \sum_{l\neq i,\sigma'} \left( t^{22}_{il} B^{22}_{i\sigma\sigma'} X^{\sigma' 2}_l - 2\sigma t^{21}_{il} B^{21}_{i\sigma\sigma'} X^{0\bar{\sigma}'}_l \right) \\ &- \sum_{l\neq i} X^{02}_i \left( t^{11}_{il} X^{\sigma 0}_l + 2\sigma t^{21}_{il} X^{2\bar{\sigma}}_l \right), \qquad (11) \end{aligned}$$

where $B^{\alpha\beta}_{i\sigma\sigma'}$ are Bose-like operators describing the number (charge) and spin fluctuations:

$$\begin{aligned} B^{22}_{i\sigma\sigma'} &= (X^{22}_i + X^{\sigma\sigma}_i)\delta_{\sigma'\sigma} + X^{\sigma\bar{\sigma}}_i \delta_{\sigma'\bar{\sigma}} \\ &= (N_i/2 + S^z_i)\delta_{\sigma'\sigma} + S^\sigma_i \delta_{\sigma'\bar{\sigma}}, \qquad (12) \\ B^{21}_{i\sigma\sigma'} &= (N_i/2 + S^z_i)\delta_{\sigma'\sigma} - S^\sigma_i \delta_{\sigma'\bar{\sigma}}\,. \end{aligned}$$

Therefore, in the Hubbard model (1), contrary to spin-fermion models where electron interaction with spin- or charge fluctuations are specified by fitting coupling constants[3], this interaction is fixed by the hopping parameters.

### B. Mean-Field Approximation

The single-particle excitations in MFA are defined by the frequency matrix (7). By using equations of motion like (11), we get the following energy spectrum for holes in two subbands

$$\begin{aligned} \varepsilon_{1,2}(\mathbf{k}) &= (1/2)[\omega_2(\mathbf{k}) + \omega_1(\mathbf{k})] \mp (1/2)\Lambda(\mathbf{k}), \\ \Lambda(\mathbf{k}) &= \{[\omega_2(\mathbf{k}) - \omega_1(\mathbf{k})]^2 + 4W(\mathbf{k})^2\}^{1/2}, \qquad (13) \end{aligned}$$

where the original excitation spectra in the Hubbard subbands and the hybridization parameter are

$$\begin{aligned} \omega_1(\mathbf{k}) &= 4t\,\alpha_1\gamma(\mathbf{k}) + 4t'\,\beta_1\gamma'(\mathbf{k}) - \mu, \\ \omega_2(\mathbf{k}) &= 4t\,\alpha_2\gamma(\mathbf{k}) + 4t'\,\beta_2\gamma'(\mathbf{k}) + \Delta - \mu, \\ W(\mathbf{k}) &= 4t\,\alpha_{12}\gamma(\mathbf{k}) + 4t'\,\beta_{12}\gamma'(\mathbf{k}). \qquad (14) \end{aligned}$$

where we omitted $t''$ contribution in (2) and introduced the renormalization parameters $\alpha_{1(2)} = Q_{1(2)}[1 + C_1/Q^2_{1(2)}]$, $\beta_{1(2)} = Q_{1(2)}[1 + C_2/Q^2_{1(2)}]$, $\alpha_{12} = \sqrt{Q_1Q_2}[1 - C_1/Q_1Q_2]$, $\beta_{12} = \sqrt{Q_1Q_2}[1 - C_2/Q_1Q_2]$. As in the Hubbard I approximation, we neglect number fluctuations $\langle \delta N_i \delta N_j \rangle_{(i\neq j)}$ but take into account contributions from the spin correlation functions for the n.n. and the n.n.n. sites:

$$C_1 = \langle \mathbf{S}_i \mathbf{S}_{i\pm a_{x/a_y}} \rangle, \quad C_2 = \langle \mathbf{S}_i \mathbf{S}_{i\pm a_x \pm a_y} \rangle. \qquad (15)$$

The renormalization of the QP spectra (13), (14) caused by strong spin correlations in the underdoped region results in suppression of the n.n. hopping which changes the shape of the spectra and reduces the bandwidth. For instance, if we consider the limiting case of the long-range AF Néel state with the n.n. correlation function $C_1 \simeq -1/4$ at half-filling, $Q_1 = Q_2 = 1/2$, we obtain $\alpha_{1(2)} = 0$. This results in complete suppression of the n.n. hopping and transformation of the spectra (14) to the n.n.n. hopping $\propto t'\gamma'(\mathbf{k})$ as was discussed in[19].

For the diagonal components of the zero-order GF (8) we have

$$G^0_{11(22)}(\mathbf{k},\omega) = \frac{Q_{1(2)}\,[1 - b(\mathbf{k})]}{\omega - \varepsilon_{1(2)}(\mathbf{k})} + \frac{Q_{1(2)}\,b(\mathbf{k})}{\omega - \varepsilon_{2(1)}(\mathbf{k})}, \qquad (16)$$

where the parameter

$$b(\mathbf{k}) = \frac{\varepsilon_2(\mathbf{k}) - \omega_2(\mathbf{k})}{\varepsilon_2(\mathbf{k}) - \varepsilon_1(\mathbf{k})} = \frac{1}{2} - \frac{\omega_2(\mathbf{k}) - \omega_1(\mathbf{k})}{2\Lambda(\mathbf{k})} \qquad (17)$$

determines the contribution due to the hybridization.

### C. Self-energy Corrections

Dyson equation (9) for the GF is convenient to write in the form

$$\hat{G}_\sigma(\mathbf{k},\omega) = \left( \omega\hat{\tau}_0 - \hat{\varepsilon}(\mathbf{k}) - \tilde{\Sigma}_\sigma(\mathbf{k},\omega) \right)^{-1} \hat{Q}, \qquad (18)$$

where the self-energy reads

$$\tilde{\Sigma}_\sigma(\mathbf{k},\omega) = \langle\langle \hat{Z}^{(ir)}_\sigma \,|\, \hat{Z}^{(ir)\dagger}_\sigma \rangle\rangle^{(prop)}_{\mathbf{k},\omega} \, \hat{Q}^{-1}. \qquad (19)$$

To make the problem tractable, we can neglect in the self-energy matrix (19) the off-diagonal components $\tilde{\Sigma}_{12,\sigma}(\mathbf{k},\omega)$ in comparison with the hybridization parameters $W(\mathbf{k})$ in (14). This enables us to write the diagonal components of the full GF (18) in the form similar to (16):

$$\begin{aligned} \hat{G}_{11(22)}(\mathbf{k},\omega) &= \frac{Q_{1(2)}\,[1 - b(\mathbf{k})]}{\omega - \varepsilon_{1(2)}(\mathbf{k}) - \tilde{\Sigma}_{11(22)}(\mathbf{k},\omega)} \\ &+ \frac{Q_{1(2)}\,b(\mathbf{k})}{\omega - \varepsilon_{2(1)}(\mathbf{k}) - \tilde{\Sigma}_{22(11)}(\mathbf{k},\omega)}\,. \qquad (20) \end{aligned}$$

Here the hybridization parameters $b(\mathbf{k})$ are determined by the formula similar to (17) which gives an accurate approximation for a small doping at $n \sim 1$.

Now we calculate the self-energy (19) in the non-crossing (NCA) or the self-consistent Born approximation (SCBA) by neglecting vertex renormalization. As follows from the equation of motion (11), the $\hat{Z}_{\sigma}^{(ir)}$ operators determined by (5) are essentially a product of a Fermi-like $X_j(t)$ and Bose-like $B_i(t)$ operators. In SCBA, the propagation of these excitations of different types in the many-particle GF in (19) are assumed to be independent of each other. Therefore, they can be decoupled in the time-dependent correlation functions for lattice sites ($i \neq j$, $l \neq m$) as follows

$$\langle B_i(t) X_j(t) B_l X_m \rangle \simeq \langle X_j(t) X_m \rangle \langle B_i(t) B_l \rangle. \qquad (21)$$

Using the spectral representation for these correlation functions, we obtain the following formula for the diagonal self-energy components $\tilde{\Sigma}_{11(22)}(\mathbf{k},\omega) = \Sigma(\mathbf{k},\omega)$ which are the same for two subbands:

$$\Sigma(\mathbf{k},\omega) = \frac{1}{N}\sum_{\mathbf{q}} \int_{-\infty}^{+\infty} \mathrm{d}z K(\omega, z|\mathbf{q}, \mathbf{k}-\mathbf{q}) \times (-1/\pi)\,\mathrm{Im}\,[G_1(\mathbf{q},z) + G_2(\mathbf{q},z)], \quad (22)$$

where the corresponding subband GFs are:

$$G_{1(2)}(\mathbf{q},\omega) = \frac{1}{\omega - \varepsilon_{1(2)}(\mathbf{q}) - \Sigma(\mathbf{q},\omega)}. \qquad (23)$$

The kernel of the integral equation (22) has the following form:

$$K(\omega, z|\mathbf{q}, \mathbf{k}-\mathbf{q}) = |t(\mathbf{q})|^2 \frac{1}{2\pi} \int_{-\infty}^{+\infty} \frac{\mathrm{d}\Omega}{\omega - z - \Omega} \times [\tanh(z/2T) + \coth(\Omega/2T)]\,\mathrm{Im}\,\chi_{sc}(\mathbf{k}-\mathbf{q}, \Omega), \quad (24)$$

where the interaction is defined by the hopping parameter $t(\mathbf{q})$ (2). The spectral density of bosonic excitations is determined by the dynamic susceptibility of the Bose-like operators $B_i(t)$ in (21) – the spin and number (charge) fluctuations:

$$\chi_{sc}(\mathbf{q},\omega) = -[\langle\langle \mathbf{S_q} | \mathbf{S_{-q}} \rangle\rangle_{\omega} + (1/4)\langle\langle \delta N_{\mathbf{q}} | \delta N_{-\mathbf{q}} \rangle\rangle_{\omega}], \quad (25)$$

where we introduced the commutator GF for the spin $\mathbf{S_q}$ and the number $\delta N_{\mathbf{q}} = N_{\mathbf{q}} - \langle N_{\mathbf{q}} \rangle$ operators.

Thus we obtain a self-consistent system of equations for the GFs (23) and the self-energy (22). A similar system of equations was obtained within the composite operator method[16]. In comparison with the $t$-$J$ model studied by us in[20], for the Hubbard model (1) we have two contributions in the self-energy (22) determined by the two Hubbard subbands, while in the $t$-$J$ model only one subband is considered. However, depending on the position of the chemical potential, a substantial contribution to the self-energy comes only from the GF of those subband which is close to the Fermi energy. A contribution from the GF of another subband which is far from the Fermi energy, is suppressed due to a large charge-transfer energy $\Delta$ in the denominator of those GF. Neglecting the latter contribution, we obtain a self-consistent system of equations for one GF close to the Fermi energy and the corresponding self-energy function similar to the $t$-$J$ model [20].

## III. RESULTS AND DISCUSSION

### A. Self-consistent system of equations

To solve the system of equations for the self-energy (22) and the GFs (23) we should specify a model for the spin-charge susceptibility (25). Below we take into account only the spin-fluctuation contribution $\chi_s(\mathbf{q},\omega) = -\langle\langle \mathbf{S}_q \mid \mathbf{S}_{-q} \rangle\rangle_{\omega}$ for which we adopt a model suggested in numerical studies[25]

$$\mathrm{Im}\,\chi_s(\mathbf{q},\omega + i0^+) = \chi_s(\mathbf{q})\,\chi_s^{''}(\omega) = \frac{\chi_0}{1 + \xi^2(1+\gamma(\mathbf{q}))}\,\tanh\frac{\omega}{2T}\frac{1}{1+(\omega/\omega_s)^2}. \quad (26)$$

The $\mathbf{q}$-dependence in $\chi_s(\mathbf{q})$ is determined by the AF correlation length $\xi$ which doping dependence is defined below. The static susceptibility $\chi_0$ at the AF wave vector $\mathbf{Q} = (\pi,\pi)$ is fixed by the normalization condition:

$$\langle \mathbf{S}_i^2 \rangle = \frac{1}{N}\sum_i \langle \mathbf{S}_i \mathbf{S}_i \rangle = \frac{1}{\pi}\int_{-\infty}^{+\infty} \frac{dz}{\exp(z/T) - 1}\chi_s^{''}(z)\,\frac{1}{N}\sum_{\mathbf{q}}\chi_s(\mathbf{q}), \quad (27)$$

which gives the following value for this constant:

$$\chi_0 = \frac{2}{\omega_s}\langle \mathbf{S}_i^2 \rangle \left\{ \frac{1}{N}\sum_{\mathbf{q}} \frac{1}{1 + \xi^2[1+\gamma(\mathbf{q})]} \right\}^{-1}. \qquad (28)$$

In (27) we introduced $\langle \mathbf{S}_i^2 \rangle = 3\langle S_i^z\, S_i^z \rangle = (3/4)\langle (1 - X_i^{00} - X_i^{22}) \rangle \simeq (3/4)(1 - |\delta|)$ where at the hole doping $\delta \simeq \langle X_i^{22} \rangle$, while at the electron doping $\delta \simeq -\langle X_i^{00} \rangle$.

The spin correlation functions (15) in the single-particle excitation spectra (13) in MFA are defined by equations

$$C_1 = \frac{1}{N}\sum_{\mathbf{q}} C_{\mathbf{q}}\,\gamma(\mathbf{q}), \quad C_2 = \frac{1}{N}\sum_{\mathbf{q}} C_{\mathbf{q}}\,\gamma'(\mathbf{q}). \qquad (29)$$

The static correlation function $C_{\mathbf{q}}$ can be calculated from the same model (26) as follows

$$C_{\mathbf{q}} = \langle \mathbf{S_q} \mathbf{S_{-q}} \rangle = \frac{C(\xi)}{1 + \xi^2[1+\gamma(\mathbf{q})]}, \qquad (30)$$

where the factor $C(\xi) = \chi_0\,(\omega_s/2)$.

TABLE I: Static spin correlation functions (29), $C(\xi)$ (30) and the AF correlation length $\xi$ in (26) at various hole concentrations $n = 1 + \delta$

| $\delta =$ | 0.03 | 0.05 | 0.10 | 0.15 | 0.20 | 0.30 |
|---|---|---|---|---|---|---|
| $C_1$ | -0.36 | -0.26 | -0.21 | -0.18 | -0.14 | -0.10 |
| $C_2$ | 0.27 | 0.16 | 0.11 | 0.09 | 0.06 | 0.04 |
| $C(\xi)$ | 22.0 | 5.91 | 3.58 | 2.67 | 1.93 | 1.40 |
| $\xi$ | 8.0 | 3.40 | 2.50 | 2.10 | 1.70 | 1.40 |

To specify the doping dependence of the AF correlation length $\xi(\delta)$ at low temperature, we fit the correlation function $C_1$ calculated from (29) to the numerical results of an exact diagonalization for finite clusters [26]. The values of the AF correlation length, calculated values of $C_2$ and the correlation function $C(\xi) = \langle \mathbf{S_q S_{-q}} \rangle$ at the AF wave-vector $\mathbf{q} = \mathbf{Q} = (\pi, \pi)$ are given in Table I.

To perform numerical calculations, we introduce the imaginary frequency representation for the GF (23):

$$G_{1(2)}(\mathbf{q}, i\omega_n) = \frac{1}{i\omega_n - \varepsilon_{1(2)}(\mathbf{q}) - \Sigma(\mathbf{q}, i\omega_n)}\,. \qquad (31)$$

where $i\omega_n = i\pi T(2n+1),\ n = 0, \pm 1, \pm 2,\ ...\ .$ For the self-energy (22) we obtain the following representation:

$$\Sigma(\mathbf{k}, i\omega_n) \ = \ -\frac{T}{N}\sum_{\mathbf{q}}\sum_{m}[G_1(\mathbf{q}, i\omega_m) + G_2(\mathbf{q}, i\omega_m)] \times \ \lambda(\mathbf{q}, \mathbf{k}-\mathbf{q} \mid i\omega_n - i\omega_m)\,. \qquad (32)$$

The interaction function is given here by the equation

$$\lambda(\mathbf{q}, \mathbf{k}-\mathbf{q} \mid i\omega_\nu) = -|t(\mathbf{q})|^2\, \chi_s(\mathbf{k}-\mathbf{q})\ F_s(i\omega_\nu), \quad (33)$$

where the spectral function:

$$F_s(\omega_\nu) = \frac{1}{\pi}\ \int_0^\infty \frac{2xdx}{x^2 + (\omega_\nu/\omega_s)^2}\ \frac{1}{1+x^2}\ \tanh\frac{x\,\omega_s}{2T}. \qquad (34)$$

Let us compare the self-consistent system of equations for the GF (31) and the self-energy (32) with results of other theoretical approaches. In our theory based on the HO technique we start from the two-subband representation for the GF (4) which rigorously takes into account strong electron correlations determined by the Coulomb energy $U_{eff}$. This results in the Mott gap at large $U_{eff}$ (see below) as in the DMFT. On the other hand, the kinematic interaction, generic to HOs, induces the electron scattering by spin (charge) dynamical fluctuations (25) which are responsible for the pseudogap formation as in the two-particle self-consistent approach (TPSC) [12,27] or the model of short-range static spin (charge) fluctuations – the $\Sigma_{\mathbf{k}}$-model[2].

To prove this, let us consider the classical limit for the self-energy (32) by taking into account only the zero Matsubara frequency $i\omega_\nu = 0$ in the interaction (33) which gives $i\omega_m = i\omega_n$ in (32). In the limit of large AF correlation length $\xi \gg 1$ the static spin susceptibility $\chi_s(\mathbf{q})$ in (26) shows a sharp peak close to the AF wave-vector $\mathbf{Q} = (\pi, \pi)$ and can be expanded over the small wave-vector $\mathbf{p} = \mathbf{q} - \mathbf{Q}$:

$$\chi_s(\mathbf{q}) \simeq \frac{\chi_0}{1 + \xi^2\,\mathbf{p}^2} \simeq \frac{A}{\kappa^2 + \mathbf{p}^2}. \qquad (35)$$

where we introduced $\kappa = \xi^{-1}$ and took into account that the constant (28) $\chi_0 \simeq A\,\xi^2$ with $A = (8\pi/\omega_s)\langle \mathbf{S}_i^2 \rangle [\ln(1 + 4\pi\,\xi^2)]^{-1}$ for the square lattice. In this limit we get the following equation for the self-energy (32):

$$\Sigma(\mathbf{k}, i\omega_n) \simeq |g(\mathbf{k}-\mathbf{Q})|^2\,\frac{T}{N}\sum_{\mathbf{p}}\frac{1}{\kappa^2 + p^2} \times [G_1(\mathbf{k}-\mathbf{Q}-\mathbf{p}, i\omega_n) + G_2(\mathbf{k}-\mathbf{Q}-\mathbf{p}, i\omega_n)], \quad (36)$$

where the effective interaction

$$|g(\mathbf{q})|^2 = A\,|t(\mathbf{q})|^2\,F_s(0). \qquad (37)$$

Expanding the QP energy $\varepsilon_{1(2)}(\mathbf{k}-\mathbf{Q}-\mathbf{p}) \simeq \varepsilon_{1(2)}(\mathbf{k}-\mathbf{Q}) - \mathbf{p}\cdot\mathbf{v}_{1(2),\mathbf{k}-\mathbf{Q}}$ we obtain for the GFs in (36) the following representation:

$$G_{1(2)}(\mathbf{k}-\mathbf{Q}-\mathbf{p}, i\omega_n) \simeq \{i\omega_n - \varepsilon_{1(2)}(\mathbf{k}-\mathbf{Q}) + \ \mathbf{p}\cdot\mathbf{v}_{1(2),\mathbf{k}-\mathbf{Q}} - \Sigma(\mathbf{k}-\mathbf{Q}, i\omega_n)\}^{-1}. \qquad (38)$$

The system of equations for the GFs (38) and the self-energy (36) is similar to those one derived in the TPSC approach[27]) and the $\Sigma_{\mathbf{k}}$-model[2] apart from the interaction function and the two-subband system of equations. In our approach the vertex (37) is determined by the hopping parameter $|t(\mathbf{k}-\mathbf{Q})|^2$, while in the TPSC and the $\Sigma_{\mathbf{k}}$-model the coupling constant is induced by the Coulomb scattering, e.g., in[15] $g^2 = U^2(\langle n_{i\uparrow} n_{i\downarrow}\rangle/n^2)\langle \mathbf{S}_i^2\rangle/3$. However, the values of these vertices are close: the averaged over the BZ value $\langle\sqrt{|t(\mathbf{k})|^2}\rangle_{\mathbf{k}} \sim 2t$ is comparable with the coupling constant $g \leq 2t$ used in[13]. In the spin-fermion model the self-energy is also determined by spin-fluctuations (see, e.g.,[3]) with the coupling constant fitted from ARPES experiments $g \sim 0.7$ eV$\sim 2t$ of the same order. As in the TPSC theory, in the limit $\xi \to \infty$ the AF gap $\Delta_{AF}(\mathbf{k}) \propto |t(\mathbf{k}-\mathbf{Q})|^2$ in the QP spectra emerges in the subband located at the Fermi energy. This result readily follows from the self-consistent equations for the GF (31) with the self-energy (36) where in the right-had side GF (38) is taken at $\mathbf{p} = 0$. Thus, in our approach the pseudogap formation is mediated by the AF short-range order similar to TPSC theory and the model of short-range static spin fluctuations in the generalized DMFT [15].

In the next sections we consider the results of self-consistent calculations of the GFs (31) and the self-energy (32) in the hole doped case for various hole concentration $\delta = n - 1 > 0$. In Sects. III B – III D the calculations were performed at temperature $T = 0.03t \simeq 140$ K and $T = 0.3t$ for $\Delta = 8t$, $t \simeq 0.4$ eV and

$t' = -0.3t$. Several results are reported for $\Delta = 4t$, $t' = -0.13t$, $t'' = 0.16t$ in Sect. III E. For the spin-fluctuation energy in (26) we take $\omega_s = 0.4t$. The AF correlation length $\xi(\delta)$ and the static correlation functions $C_1, C_2$ in (15) are defined in Table I.

### B. Dispersion and spectral functions

In ARPES measurements and QMC simulations the spectrum of single-electron excitations is determined by the spectral function $A_{(el)}(\mathbf{k},\omega) = A_{(h)}(\mathbf{k},-\omega)$. The spectral function for holes can be written as follow:

$$A_{(h)}(\mathbf{k},\omega) = -\frac{1}{\pi}\,\mathrm{Im}\,\langle\langle a_{\mathbf{k}\sigma} \mid a^{\dagger}_{\mathbf{k}\sigma}\rangle\rangle_{\omega+i0^+}$$
$$= [Q_1 + P(\mathbf{k})]A_1(\mathbf{k},\omega) + [Q_2 - P(\mathbf{k})]A_2(\mathbf{k},\omega). \quad (39)$$

Here we introduced for the hole annihilation $a_{\mathbf{k}\sigma}$ and creation $a^{\dagger}_{\mathbf{k}\sigma}$ operators the definition in terms of the Hubbard operators $a_{\mathbf{k}\sigma} = X^{0\sigma}_i + 2\sigma X^{\bar{\sigma}2}_i$, $a^{\dagger}_{\mathbf{k}\sigma} = X^{\sigma 0}_i + 2\sigma X^{2\bar{\sigma}}_i$ and used all four components of the matrix GF (18) $\hat{G}_{\alpha\beta}(\mathbf{k},\omega)$ with the diagonal components given by (20). In (39) we introduced also the one-band spectral functions determined by the GFs (23): $A_{1(2)}(\mathbf{k},\omega) = -(1/\pi)\,\mathrm{Im}G_{1(2)}(\mathbf{q},\omega)$. The hybridization effects are allowed for by the parameter $P(\mathbf{k}) = (n-1)b(\mathbf{k}) - 2\sqrt{Q_1 Q_2}\,W(\mathbf{k})/\Lambda(\mathbf{k})$.

The dispersion curves given by maxima of spectral functions (39) were calculated for hole doping $\delta = 0.05 - 0.3$. At low hole doping, $\delta = 0.05, 0.1$, the dispersion reveal a rather flat hole-doped band at the Fermi energy (FE) ($\omega = 0$) as shown in the upper panel in Fig. 1. The corresponding spectral function (the bottom panel) demonstrates weak QP peaks at the Fermi energy. With doping, the dispersion and the intensity of the QP peaks at the Fermi energy substantially increase as demonstrated in Fig. 2 though a flat band in $X(\pi,0) \to \Gamma(0,0)$ direction is still observed in accordance with ARPES measurements in the overdoped $La_{1.78}Sr_{0.22}CuO_4$[28]. To study an influence of AF spin-correlations on the spectra, we calculate the spectral functions at high temperature $T = 0.3t$ for $\delta = 0.1$ by neglecting spin correlation functions (15) in the single-particle excitation spectra (13) in MFA and taking a small AF correlation length ($\xi = 1.0$) in the spin-susceptibility (26). Figure 3 shows a strong increase of the dispersion and the intensity of the QP peaks at the Fermi energy as in the overdoped region, $\delta = 0.3$, which proves a strong influence of AF spin-correlations on the spectra. A crude estimation of the Fermi velocity from the dispersion curve in the $\Gamma(0,0) \to M(\pi,\pi)$ direction in Fig. 2 for the overdoped case gives the value $V_F \simeq 7.5t$ Å $\simeq 3$ (eV·Å) for the hopping parameter $t = 0.4$ eV which can be compared with experimental results $V_F \simeq 2.2$ (eV·Å) for overdoped $La_{1.78}Sr_{0.22}CuO_4$[28] and $V_F \simeq 3.9$ (eV·Å) for overdoped Bi-2212[29]. With doping, the electronic density of states (DOS) shows a weight transfer from the upper one-hole subband to the lower two-hole singlet subband as shown in Fig. 4. However, even in the overdoped case a noticeable part of the DOS retains in the upper one-hole subband.

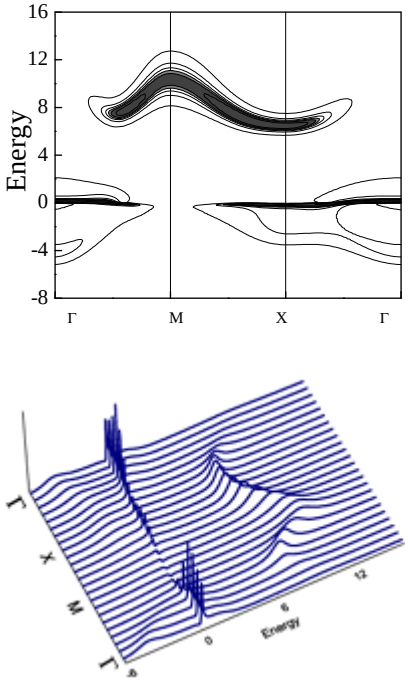


FIG. 1: Dispersion curves (upper panel) and spectral functions (bottom panel) in units of $t$ along the symmetry directions $\Gamma(0,0) \to M(\pi,\pi) \to X(\pi,0) \to \Gamma(0,0)$ for $\delta = 0.05$.

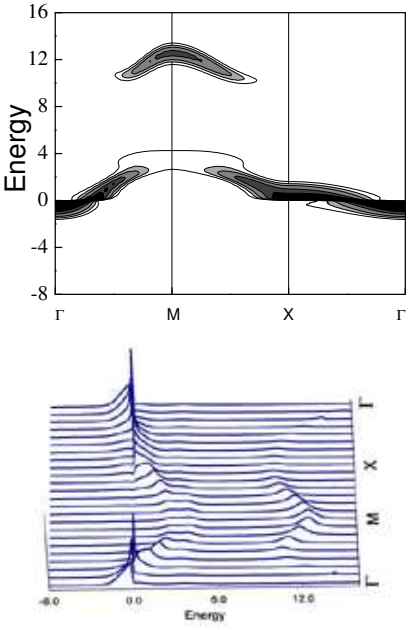


FIG. 2: The same as Fig. 1 for hole concentration $\delta = 0.3$.

It is interesting to compare our results with those obtained in the generalized DMFT[13] which should be close to each other as discussed at the end of Sect. III A.

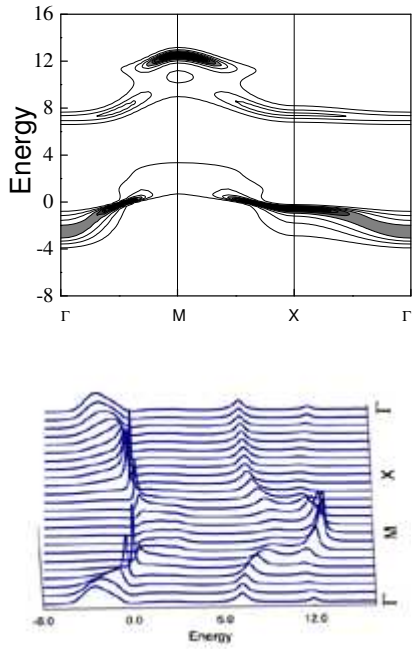


FIG. 3: The same as Fig. 1 but for the hole concentration $\delta = 0.1$ and at high temperature $T = 0.3t$.

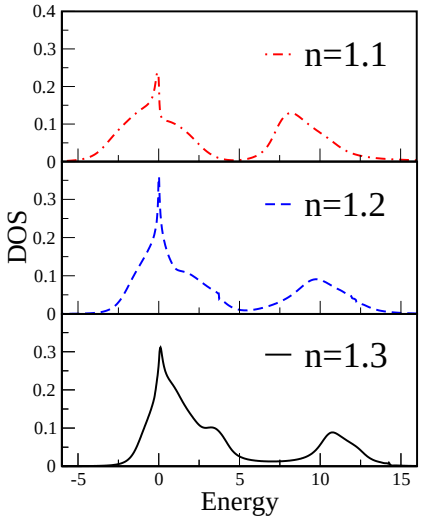


FIG. 4: (Color online) Doping dependence of the electronic density of states.

In fact, the spectral function shown in Fig. 8 in[13] for $t' = -0.4$ demonstrates a similar flat QP bands in $\Gamma(0,0) \to X(\pi,0)$ and $\Gamma(0,0) \to M(\pi,\pi)$ directions, as in our Fig. 1 and Fig. 2, a strong intensity transfer from the lower electronic Hubbard band (LHB) to the upper Hubbard band (UHB) at the $M(\pi,\pi)$ point of the BZ and a splitting of the LHB close to the $X(\pi,0)$ point. An analogous temperature and doping ($\xi$) behavior of the spectral functions and the pseudogap revealed in the both theories supports the spin-fluctuation scenario of the pseudogap formation. A similar behavior was observed also in the cluster perturbation theory[12] (see Fig. 2 (a) in[31]).

### C. Fermi surface and occupation numbers

The Fermi surface for the two-hole subband was determined by a conventional equation:

$$\varepsilon_2(\mathbf{k}_F) + \mathrm{Re}\,\Sigma(\mathbf{k}_F, \omega = 0) = 0, \qquad (40)$$

as shown in Fig. 5, and then compared with those one obtained from maxima of the spectral function $A_{el}(\mathbf{k}, \omega = 0)$ on the $(k_x, k_y)$-plane for $\delta = 0.1, 0.2$ shown in Fig. 6. The FS changes from a hole arc-type at $\delta = 0.1$ to an electron-like one at $\delta = 0.3$. Experimentally an electron-like FS was observed in the overdoped $La_{1.78}Sr_{0.22}CuO_4$[28]. The doping dependent FS transformation can be also observed by studying the electron occupation numbers. The electron occupation numbers in $(\mathbf{k})$-space for one spin-direction equal to $N_{(el)}(\sigma, \mathbf{k}) = 1 - N_{(h)}(\sigma, \mathbf{k})$ where the hole occupation numbers $N_{(h)}(\sigma, \mathbf{k}) \equiv N_{(h)}(\mathbf{k})$ according to (3) are determined only by the diagonal GFs (20). From the latter

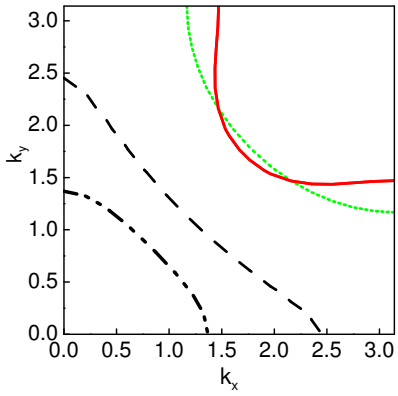


FIG. 5: (Color online) Doping dependence of the FS for $\delta = 0.1$ (full line at $T = 0.03t$ and dotted line at $T = 0.3t$), $\delta = 0.2$ (dashed line), and $\delta = 0.3$ (dot-dashed line).

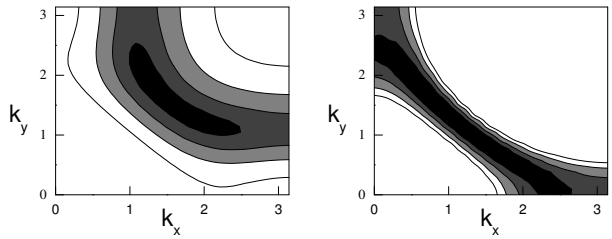


FIG. 6: $A(\mathbf{k}, \omega = 0)$ on the FS for $\delta = 0.1$ (left panel), $\delta = 0.2$ (right panel).

equation and (23) we get:

$$
\begin{aligned}
N_{(h)}(\mathbf{k}) &= [Q_1 + (n-1)b(\mathbf{k})]\, N_1(\mathbf{k}) \\
&+ [Q_2 - (n-1)b(\mathbf{k})\, N_2(\mathbf{k}), \\
N_{1(2)}(\mathbf{k}) &= -\frac{1}{\pi}\int_{-\infty}^{\infty} \frac{d\omega}{e^{\omega/T}+1}\, \mathrm{Im}\, G_{1(2)}(\mathbf{k},\omega) \\
&= \frac{1}{2} + \frac{T}{2}\sum_{m=-\infty}^{\infty} G_{1(2)}(\mathbf{k}, i\omega_m). \qquad (41)
\end{aligned}
$$

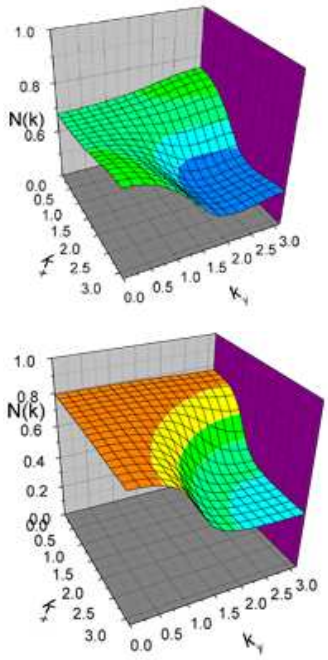


FIG. 7: (Color online) The electronic occupation numbers $N_{\mathbf{k}}$ for $\delta = 0.1$ at $T = 0.03t$ (upper panel) and at $T = 0.3t$ (bottom panel).

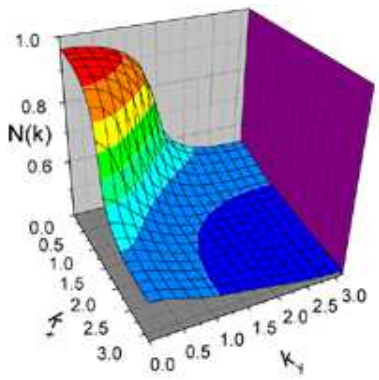


FIG. 8: (Color online) The electronic occupation numbers $N_{\mathbf{k}}$ at $T = 0.03t$ for $\delta = 0.3$.

The electron occupation numbers in a quarter of the BZ $(0 < k_x, k_y < \pi)$ are shown in Fig. 7 for $\delta = 0.1$ at low temperature $T = 0.03t$ and at high temperature $T = 0.3t$. With doping the the shape of the $N_{\mathbf{k}}$ is changing revealing a transition of the hole-like FS to the electron-like in the overdoped case $\delta = 0.3$ as plotted in Fig. 8.

While in the underdoped case at $\delta = 0.1$ the drop of the occupation numbers at the Fermi level crossing is rather small, $\Delta N_{(el)} \simeq 0.15$, for high temperature $T = 0.3t$ or in the overdoped case at $\delta = 0.3$ when the AF spin correlations are suppressed, the occupation number drops are substantially increased: $\Delta N_{(el)} \simeq 0.45, 0.55$, respectively. Thus, the arc formation and a small change of the electron occupation numbers at the FS crossing at low doping further prove a large contribution of the spin correlations in the renormalization of QP spectra.

The obtained result concerning the "destruction" of the FS caused by the arc formation shown in Fig. 6 and Fig. 16 for low doping, which corresponds to large $\xi$, correlates well with the studies within the generalized DMFT[14]. As shown in Fig. 2 in[14], the spectral density intensity plots clearly demonstrate the arc formation on the FS for large coupling constant $\lambda_{sf} = \Delta = 2t$ and $\xi = 10$, while the FS determined from (40) gives several solutions as in our Fig. 15 for $U_{eff} = 4\,t$ in Sect. III E.

### D. Self-energy and kinks

Energy dependence of the real and imaginary parts of the self-energy $\Sigma(\mathbf{k},\omega)$ for $\delta = 0.1, 0.3$ at the $\Gamma(0,0)$, $S(\pi/2,\pi/2)$ and $M(\pi,\pi)$ points are shown in Fig. 9. These plots demonstrate a strong dependence of the self-energy on the wave-vector and the hole concentrations. With doping, the coupling constant substantially decreases as seen by the decreasing of the imaginary part and the slope of the real part at the FS crossing which determines the coupling constant $\lambda = -(\partial\, \mathrm{Re}\tilde{\Sigma}(\mathbf{k},\omega)/\partial\omega)_{\omega=0}$. As shown in Fig. 10, the coupling constant in the $\Gamma(0,0) \rightarrow M(\pi,\pi)$ direction decreases from $\lambda \simeq 7.86$ at $\delta = 0.1$ to $\lambda \simeq 3.3$ at $\delta = 0.3$.

At large binding energies (greater than the boson energy responsible for the interaction) the self-energy effects vanish and the electron dispersion should return to the bare value, giving a sharp bend, the so-called "kink" in the electron dispersion. The amplitude of the kink and the energy scale where it occurs are related to the strength of the electron-boson interaction and the boson energy, respectively. In ARPES the kink is observed as a changing of the slope for an intensity plot for the spectral function $A(\mathbf{k},\omega)$ in a particular $\mathbf{k}$-wave vector direction below the Fermi level $\omega \leq 0$ (for electrons). Usually two directions are studied: the nodal $(\Gamma \rightarrow M)$ and the antinodal $(X \rightarrow M)$ ones. Intensity plots for the spectral function $A(\mathbf{k},\omega)$ at $\delta = 0.1$ are shown in Fig. 11 in the nodal direction (left panel) and the antinodal one (right panel). The same plots at $\delta = 0.3$ are shown in Fig. 12 in the nodal direction (left panel) and $X(\pi,0) \rightarrow \Gamma(0,0)$

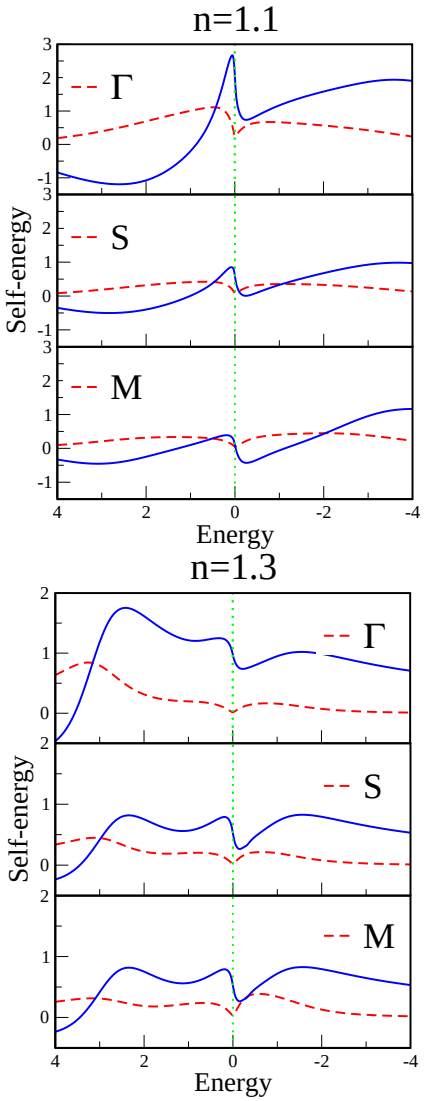


FIG. 9: (Color online) Energy dependence of the real and imaginary parts of the self-energy $\Sigma(\mathbf{k},\omega)$ at the $\Gamma(0,0)$, $S(\pi/2,\pi/2)$ and $M(\pi,\pi)$ points at $\delta = 0.1$ (upper panel) and $\delta = 0.3$ (bottom panel).

direction (right panel). A change of dispersion is clearly seen with increasing binding energy below the FS shown by dotted line. For the underdoped case the kink is larger than for the overdoped one. A crude estimation of the strength of the kink from the ratio of the dispersion slope $V_{\rm F}$ close to the FS ($\omega = 0$) to those one $V_{\rm F}^0$ at large binding energy ($\omega \sim 0.2t$), $V_{\rm F}^0/V_{\rm F} = (1+\lambda)$, gives the following values: $(1+\lambda) \sim 7.6$, 3.5 at $\delta = 0.1$ for the nodal and antinodal directions, respectively. In the overdoped case the nodal value is much smaller, while in the the antinodal $X(\pi,0) \to \Gamma(0,0)$ direction is still quite large: $(1+\lambda) \sim 2.5$. These estimations are in accord with the evaluation of the coupling constant $\lambda$ from the slope of the real part of the self-energy discussed above.

It is important to stress that in our theory the self-energy effects and the corresponding kinks are induced

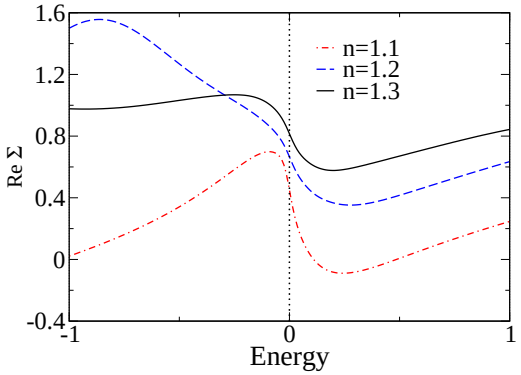


FIG. 10: (Color online) $\mathrm{Re}\Sigma(\mathbf{k},\omega)$ in the $\Gamma(0,0) \to M(\pi,\pi)$ direction at the FS.

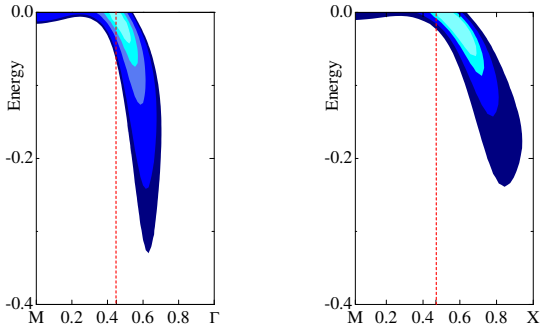


FIG. 11: (Color online) Dispersion curves along the symmetry directions $M(\pi,\pi) \to \Gamma(0,0)$ (left panel) and $M(\pi,\pi) \to X(\pi,0)$ (right panel) in units of $t$ for $\delta = 0.1$, $T = 0.03t$. Fermi level crossing is shown by vertical dotted line.

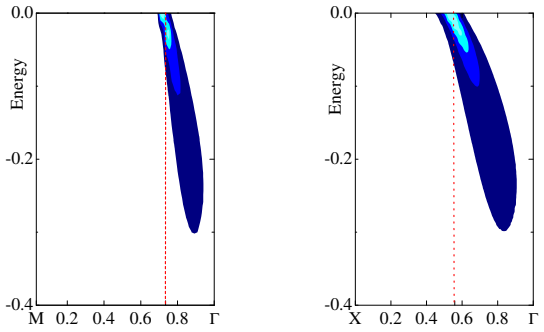


FIG. 12: (Color online) The same as Fig. 11 but for $\delta = 0.3$ along the symmetry directions $M(\pi,\pi) \to \Gamma(0,0)$(left panel) and $X(\pi,0) \to \Gamma(0,0)$ (right panel).

by the spin-fluctuation spectrum in the form of the continuum (26) which at low temperature $T \sim 0.03t \ll \omega_s = 0.4t$ has a large intensity already at small energy $\omega \sim 0.03t$ and decreases slowly up to a high energy

$\omega \sim t$. In the spin-fermion model the kink phenomenon is usually explained by electron interaction with the spin-resonance mode $\Omega_{\rm res} \simeq 40$ meV observed in the superconducting state. This results in a break of the electron dispersion ("kink") at a certain energy $\omega \sim \Omega_{\rm res} + \Delta_0$ where $\Delta_0$ is the superconducting gap (see, e.g.[3]). In the normal state considered in our theory the spin-resonance mode is inessential. Its contribution amounting only few percents of the total spin fluctuation spectrum (27) should not change our results which reveal a rather strong interaction with a smooth energy variation without any specific kink energy.

### E. Dispersion and FS at $U_{\rm eff} = \Delta = 4t$

The effective Coulomb energy in the Hubbard model (1) $U_{eff} = 8t$ results in a large charge-transfer gap $\Delta \simeq 3$ eV for $t = 0.4$ eV even in the overdoped case, Fig. 2, while experiments point to a smaller value of the order of $1.5 - 2$ eV. To correct this inconsistency, we present in this section the results obtained for a smaller value of $U_{eff} = \Delta = 4t$. We also take into account the hoping parameter for the n.n.n. $\pm 2a_x, \pm 2a_y$ sites and fix the hoping parameter in the model dispersion (2) as suggested for the effective Hubbard model based on the tight-binding fitting the LDA calculations for $La_2CuO_4$[30] as follow: $t' = -0.13t$, $t'' = 0.16t$ with $t \simeq 0.7$ eV.

Main results for the dispersion and the spectral functions are not changed much in comparison with the previous ones as shown in Fig. 13. Larger hybridization between the subbands at small value of $U_{eff}$ results in increase of the dispersion and the intensity of the upper one-hole subband. This trend is also seen in the DOS in Fig. 14. At weak doping the Mott gap between the subbands is observed despite the intermediate Coulomb energy $U_{eff} = 4t$, only a half of the bare bandwidth $W \simeq 8t$. This can be explained by a reduction of the bandwidth caused by strong spin correlations in the underdoped region up to $\tilde{W} \sim 8|t'|$ as discussed in Sect. II B, below the equation (15). In the overdoped case at $\delta = 0.3$ when the spin correlations become weak the gap between the subbands vanishes.

Noticeable changes are observed for the FS shown in Fig. 15 and in Fig. 16. In the first plot where the FS was determined by the equation (40) we see a large pocket at small doping $\delta = 0.1$ which opens with doping or temperature increase. At the overdoping for $\delta = 0.3$, the FS transforms to the electron-like as in the previous calculations. This transformation is confirmed by calculations of the electron occupation numbers shown in Fig. 17. It should be noted that a pronounced hole pocket in the new set of the model parameters is caused by the $t''$ contribution which results in a large dispersion in the $(\pi, 0) \to (0, \pi)$ direction ($\propto t''(\cos 2k_x + \cos 2k_y)$) disregarded in the previous set of the parameters. A remarkable feature of these results is that the part of the FS close to the $\Gamma(0,0)$ point in the nodal direction in

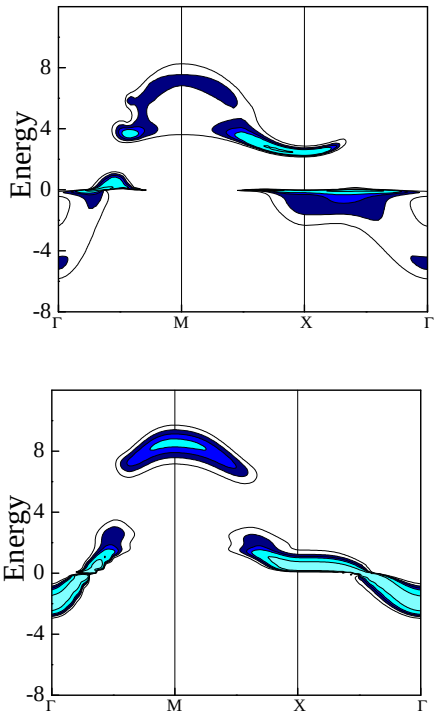


FIG. 13: (Color online) Dispersion curves for $\Delta = 4t$ along the symmetry directions $\Gamma(0,0) \to M(\pi,\pi) \to X(\pi,0) \to \Gamma(0,0)$ at $\delta = 0.05$ (upper panel) and $\delta = 0.3$ (bottom panel).

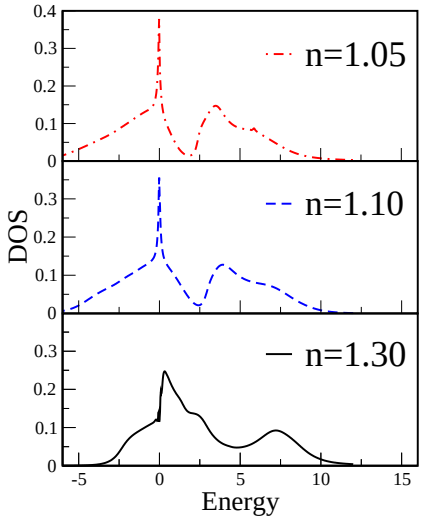


FIG. 14: (Color online) Doping dependence of the DOS for $\Delta = 4t$.

Fig. 15 does not shift much with doping (or temperature) being pinned to a large FS as observed in ARPES experiments (see, e.g.[29]). In fact, only this part of the FS was detected in ARPES experiments where the spectral

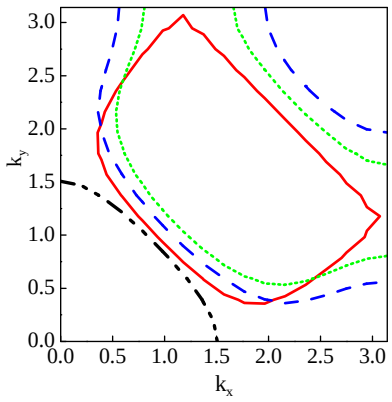


FIG. 15: (Color online) Doping dependence of the FS for $\delta = 0.1$ (full line at $T = 0.03t$ and dotted line at $T = 0.3t$), $\delta = 0.2$ (dashed line), and $\delta = 0.3$ (dot-dashed line) for $\Delta = 4t$.

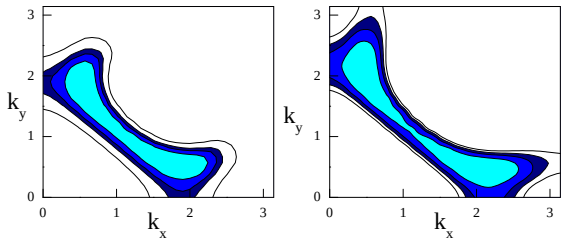


FIG. 16: (Color online) $A(\mathbf{k}, \omega = 0)$ on the FS at $\delta = 0.05$ (left panel) and $\delta = 0.1$ (right panel) at $T = 0.03t$ for $\Delta = 4t$.

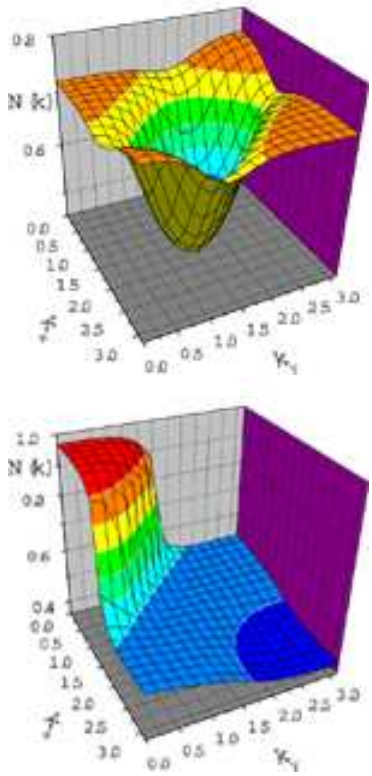


FIG. 17: (Color online) The electronic occupation numbers $N_{\mathbf{k}}$ at $T = 0.03t$ for $\delta = 0.05$ (upper panel) and at $\delta = 0.3$ (bottom panel) for $\Delta = 4t$.

function $A_{el}(\mathbf{k}, \omega = 0)$ shown in Fig. 16 was measured.

Concerning the self-energy effects and kinks, they are similar to the case for $\Delta = 8t$ and confirm a strong influence of spin correlations on the QP spectra renormalization. As shown in Fig. 18, the coupling constant $\lambda = -(\partial \mathrm{Re}\tilde{\Sigma}(\mathbf{k}, \omega)/\partial\omega)_{\omega=0}$ being large at small doping distinctly decreases with overdoping at $\delta = 0.3$ accompanied by suppression of the imaginary part of the self-energy. In conclusion, the alternative set of parameters with a moderate effective Coulomb energy $U_{eff} = 4t$ in the Hubbard model (1) confirms an important role of AF correlations in the electronic structure of system with large single-site Coulomb interaction.

## IV. CONCLUSION

In the present paper the theory of electronic spectra in the strong correlation limit for the Hubbard model (1) in a paramagnetic state has been formulated. By employing the Mori-type projection technique for the thermodynamic GFs in terms of the Hubbard operators, we consistently took into account charge carrier scattering by dynamical spin fluctuations and derived the self-consistent system of equations for the GF (23) and the self-energy (22) evaluated in the NCA which neglects the vertex corrections. Though in the Hubbard model (1) the electron coupling to spin-fluctuations is not weak, it is of the order of the hopping parameter, the vertex corrections should not be so important in this case due to kinematic restrictions imposed on the spin-fluctuation scattering. As was shown for the $t$-$J$ model[32], the leading two-loop crossing diagram identically vanishes, while the next three-loop crossing diagram gives a small contribution to the self-energy. In any case, the NCA for the self-energy can be considered as a starting approximation for a model with strong coupling. As we discussed at the end of Sect. III A, the self-consistent system of equations for the self-energy in the classical limit in our approach are similar to the two-particle self-consistent approach (TPSC)[27] or the model of short-range static spin (charge) fluctuations[15]. Numerical results for the spectral density and the FS in the NCA approximation for the self-energy are quite similar to the studies within the generalized DMFT[13,15] where all diagrams for electron scattering by spin (or charge) fluctuations in the static approximation were taken into account. Our results are also in accord with calculations based on the cluster approximation[12] and the TPSC[27].

In the present paper we have not presented a fully self-

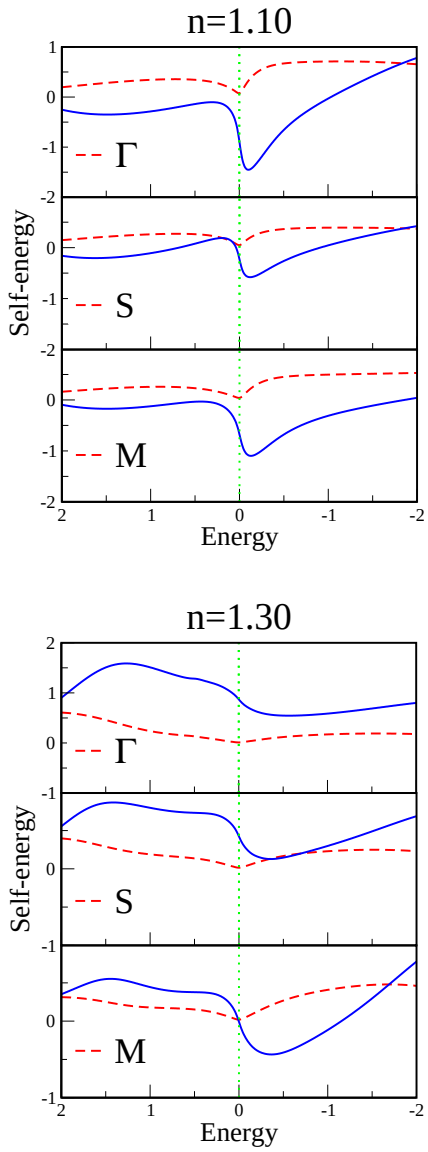


FIG. 18: (Color online) Energy dependence of the real and imaginary parts of the self-energy $\Sigma(\mathbf{k},\omega)$ for $\Delta = 4t$ at the $\Gamma(0,0)$, $S(\pi/2,\pi/2)$ and $M(\pi,\pi)$ points at $\delta = 0.1$ (upper panel) and $\delta = 0.3$ (bottom panel).

consistent theory for the single-electron GF and the dynamical spin and charge susceptibility. This demands rather involved calculations of the collective spin and charge excitation spectra which is beyond the scope of the present paper. Instead, we have used a model for the dynamical spin susceptibility (26) which is usually employed in phenomenological approach. However, a variation of the electron (hole) interaction with spin fluctuations in our theory is strongly restricted since the vertex of the interaction is given by the hopping parameters (2) in the Hubbard model, while an intensity of spin fluctuations at the AF wave-vector $\mathbf{Q}$ ($C(\xi)$ in the Table I) determined by the AF correlation length $\xi$ is fixed by the sum rule (27). A variation of the cut-off energy $\omega_s$ does not affect noticeably the numerical results, as we have checked. The resulting coupling constant $\lambda$ obtained in our calculations (see Sect. III D) seems to be too large in comparison with ARPES results. This discrepancy can be caused by disregarding scattering on charge fluctuations in the dynamical susceptibility model (25) and electron-phonon interaction which may reduce the contribution from the electron-spin interaction.

The main conclusion of the present study is that a decisive role in renormalization of the electronic spectrum in strongly correlated system as cuprate superconductors is played by electron interaction with spin-fluctuations which is in accord with other studies (e.g.,[3,12,15]). The numerical results for the electron dispersion in Sect. III B, the FS and the occupation numbers in Sect. III C, and the self-energy in Sect. III D unambiguously approved this conclusion. With doping or temperature increasing, spin correlations are suppressed which results in transition from a strong to a weak correlation limit. These observations were confirmed also by a consideration of the model with intermediate Coulomb correlations in Sect. III E.

A theory of superconducting transition within the present theory will be considered elsewhere.

### Acknowledgments

One of the authors (N.P.) is grateful to Prof. P. Fulde for the hospitality extended to him during his stay at MPIPKS, Dresden, where a major part of the present work has been done.

[1] A. Damascelli, Z. Hussain, and Z.-X. Shen, Rev. Mod. Phys. **75**, 473 (2003).
[2] M.V. Sadovskii, Usp. Phys. Nauk **171**, 539 (2001) [Physics-Uspekhi **44**, 515 (2001)].
[3] M. Eschrig, Advances in Physics **55**, 47 (2006).
[4] P.W. Anderson, Science **235**, 1196 (1987); P.W. Anderson, *The theory of superconductivity in the high-$T_c$ cuprates*. Princeton University Press, Princeton (1997).
[5] J. Hubbard, Proc. Roy. Soc., **A 276**, 238 (1963); ibid, **A 284**, 401 (1964).
[6] N. Bulut, Advances in Physics **51**, 1587 (2002).
[7] G. Ovchinnikov and V. V. Valkov, *Hubbard Operators in the Theory of Strongly Correlated Electrons*, Imperial College Press, London, (2004).
[8] F. Mancini and A. Avella, Advances in Physics **53**, 537 (2004).
[9] A. Georges, G. Kotliar, W. Krauth, and M. Rozenberg, Rev. Mod. Phys. **68**, 13 (1996).

[10] G. Kotliar, S. Y. Savrasov, K. Haule, V.S. Oudovenko, O. Parcollet, and C.A. Marianetti, Rev. Mod. Phys. (to be published), cond-mat/0511085.
[11] Th. Maier, M. Jarrel, Th. Pruschke, and M.H. Hettler, Rev. Mod. Phys. **77**, 1027 (2005).
[12] A-M.S. Tremblay, B. Kyung and D. Sénéchal, Fizika Nizkikh Temperatur (J. Low Temp. Phys.) **32**, 561 (2006).
[13] M.V. Sadovskii, I.A. Nekrasov, E.Z. Kuchinskii, Th. Pruschke, and V.I. Anisimov, Phys. Rev. B **72**, 155105 (2005).
[14] E.Z. Kuchinskii, I.A. Nekrasov, M.V. Sadovskii, Pis'ma v Zh. Exp. Teor. Fiz. **82**, 217 (2005) [JETP Letters **82**, 198 (2005)].
[15] E.Z. Kuchinskii, I.A. Nekrasov, M.V. Sadovskii, Fizika Nizkikh Temperatur (J. Low Temp. Phys.) **32**, 528 (2006).
[16] S. Krivenko, A. Avella, F. Mancini, and N. Plakida, Physica B **359-361**, 666 (2005).
[17] Y. Kakehashi and P. Fulde, Phys. Rev. B **70**, 195102 (2004); J. Phys. Soc. Jpn. **74**, 2397 (2005).
[18] D.N. Zubarev, Usp. Fiz. Nauk, **71**, 71 (1960) [Sov. Phys. Uspekhi **3**, 320 (1960)].
[19] N.M. Plakida, R. Hayn and J.-L. Richard, Phys. Rev. B **51**, 16599 (1995).
[20] N.M. Plakida and V.S. Oudovenko, Phys. Rev. B **59**, 11949 (1999).
[21] N.M. Plakida, L. Anton, S. Adam, and Gh. Adam, Zh. Exp. Theor. Fyz **124**, 367 (2003), (JETP **97**, 331 (2003)).
[22] L.F. Feiner, J.H. Jefferson, and R. Raimondi, Phys. Rev. B **53**, 8751 (1996).
[23] V.Yu. Yushankhai, V.S. Oudovenko, and R. Hayn, Phys. Rev. B, **55**, 15562 (1997).
[24] V.J. Emery, Phys. Rev. Lett., **58**, 2794 (1987); C.M. Varma, S. Schmitt-Rink, and E. Abrahams, Solid State Commun. **62**, 681 (1987).
[25] J. Jaklič and P. Prelovśek, Phys. Rev. Lett. **74**, 3411 (1995); *ibid.* **75**, 1340 (1995).
[26] J. Bonca, P. Prelovśek, and I. Sega, Europhys. Lett. **10**, 87 (1989).
[27] Y. Vilk and A.-M. Tremblay, J. Phys. Chem. Solids (UK) **56**, 1769 (1995).
[28] T. Yoshida, X.J. Zhou, M. Nakamura, et al. Phys. Rev. B **63** 220501, (2001).
[29] A.A. Kordyuk, S.V. Borisenko, A. Koitzsch, J. Fink, M. Knupfer, and H. Berger, Phys. Rev. B **71**, 214513 (2005).
[30] M.M. Korshunov, V.A. Gavrichkov, S.G. Ovchinnikov, I.A. Nekrasov, Z.V. Pchelkina, and V.I. Anisimov, Phys. Rev. B, **72**, 165104 (2005).
[31] D. Senechal1 and A.-M. S. Tremblay, Phys. Rev. Lett. **92**,126401 (2004).
[32] Z. Liu and E. Manousakis, Phys. Rev. B **45**, 2425 (1992).